

## Turbulent Transport in Spherical Tokamaks with Transport Barriers

J.W. Connor 1), C.M. Roach 1), R.J. Hastie 1), P. Helander 1), T.J. Martin 1),  
D.J. Applegate 2), N. Joiner 3), M. Reshko 4), S. Saarelma 1), W.D. Dorland 5),  
S.C. Cowley 2) 6), S. Newton 7) and A.R. Field for the MAST Team 1)

1) Euratom/UKAEA Fusion Association, Culham Science Centre, Abingdon, UK

2) Department of Physics, Imperial College, London, UK

3) Plasma Physics Laboratory, University of Saskatchewan, Canada

4) Department of Physics, University of York, UK

5) Department of Physics, University of Maryland, USA

6) Department of Physics and Astronomy, UCLA, USA

7) H.H. Wills Physics Laboratory, University of Bristol, UK

e-mail contact of main author: [jack.connor@ukaea.org.uk](mailto:jack.connor@ukaea.org.uk)

**Abstract.** The microstability of MAST discharges L mode and H-mode discharges are analysed using the electromagnetic flux-tube GS2 code supported by interpretations using simpler analytic models. Analytic approaches are used to discuss effects of steep gradients and rotation shear, relevant to internal transport barriers. Nonlinear simulations of electron temperature gradient transport in MAST are compared with experiment.

### 1. Introduction

Spherical tokamaks (STs) have an aspect ratio  $R/a \sim 1$  (where  $R$  is the major radius and  $a$  is the minor radius) which is lower than in conventional devices where  $R/a \sim 3$ . Among various ST experiments around the world, MAST at Culham carries  $\sim 1$  MA of plasma current. In ST experiments ion heat transport frequently lies close to the level predicted by neoclassical theory, and internal transport barriers in ion and electron channels have been reported. The NSTX experiment at PPPL has found that the dominant heat transport losses usually occur through the electron channel. It is important to ask whether these experimental observations can be understood theoretically.

Microinstabilities are plasma perturbations with wavelengths perpendicular to the magnetic field approaching the ion or electron Larmor radius ( $\rho_i$  and  $\rho_e$  respectively), and are widely believed to cause anomalous transport in magnetised plasmas. The gyrokinetic equations provide the appropriate mathematical model to describe microinstabilities, and are exploited in analytical and numerical calculations. ST geometry exaggerates properties of conventional tokamaks that have important influences on microstability. Studying microstability and microturbulence in STs: (i) contributes to testing and improving existing transport theories for tokamaks in challenging regimes, (ii) improves our understanding of microinstabilities in STs and (iii) assists the optimization of confinement in STs towards the goal of a burning plasma.

There has been considerable interest over the appearance of internal transport barriers (ITBs) in tokamak plasmas, including in STs. ITBs enhance confinement by generating an insulating layer in the core region, and it is important to improve our understanding of their onset. Equilibrium plasma rotation is believed to be important in the generation of ITBs, and is therefore an important ingredient in models.

Section 2 reviews the major findings from recent microstability analyses of ST plasmas using the GS2 code [1], and includes attempts to understand some of these results analytically. Section 3 discusses theories which have been developed to improve our understanding of

ITBs, and the inclusion of equilibrium rotation in such calculations. Section 4 describes nonlinear microturbulence calculations to determine the transport arising from electron temperature gradient driven (ETG) turbulence in plasma conditions typical of the MAST experiment. Finally conclusions are presented in Section 5.

## 2. Microinstabilities

Gyrokinetic microstability calculations have been performed for plasmas which are typical of MAST [2,3] using the initial value GS2 code. GS2 has a domain that follows equilibrium magnetic field lines and comprises a narrow flux-tube of plasma. Microstability and turbulence calculations commonly include only the perturbed electrostatic potential, but GS2 can also include the full magnetic perturbation. Equilibrium sheared flows are not included in GS2, and are likely to be important when equilibrium shearing rate  $\omega_{se}$  becomes comparable with the maximum growth rate. Linearly GS2 computes the real frequency,  $\omega$ , and growth rate,  $\gamma$ , of the fastest growing instability for a prescribed perpendicular wavelength  $k_y$ , where the  $y$  direction lies perpendicular to the equilibrium field and in the magnetic flux surface, and  $x$  is the radial perpendicular direction.

Microstability analyses have been performed for equilibria from the current flat-top of two similar sawtooth-free MAST discharges: an H-mode discharge #8500 and an L-mode discharge #8505. Profiles differ substantially between the L-mode and the H-mode equilibria: the L-mode has steeper density and pressure profiles in the core region but flatter in the edge. Several interesting observations emerged from these analyses.

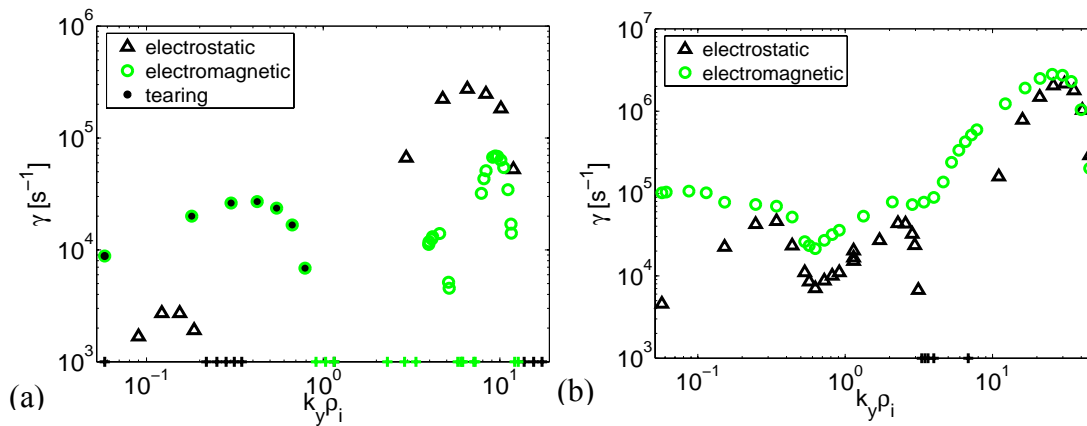


Figure 1: Growth rate of the fastest growing mode as a function of  $k_y \rho_i$  for equilibrium quantities taken from the MAST (a) H-mode flux surface at  $\rho_n = 0.4$  and (b) L-mode flux surface  $\rho_n = 0.5$ . ( $\rho_n$  is the normalised square root toroidal flux coordinate.) Results are presented with (open triangles) and without (open circles) the perturbed magnetic field. Black dots denote tearing parity modes.

Including the self-consistent magnetic perturbation makes significant modifications to the fastest growing modes. Figure 1 shows the growth rate of the fastest growing mode as a function of  $k_y$  for a core flux surface in each of these discharges.  $\beta \sim 0.1$  is moderate on both surfaces, and calculations have been performed with and without the magnetic perturbation  $\delta \mathbf{B}$ . In the H-mode plasma when  $\delta \mathbf{B}$  is included: at long wavelength ( $k_y \rho_i < 1$ ) tearing parity instabilities dominate over electrostatic ion temperature gradient (ITG) driven modes (see Figure 1(a)) and rotate in the electron diamagnetic drift direction; and at short wavelength  $k_y \rho_i \sim O(1)$  the growth rates of ETG instabilities are modified. In the L-mode case the most striking impact of including electromagnetic effects is the emergence of strongly

electromagnetic twisting parity modes for  $k_y \rho_i < 1$ . A scan in  $\beta$  (Figure 2) reveals that  $\beta$  sits close to the critical value for the onset of kinetic ballooning modes (KBM). MHD stability analysis suggests that this surface is just beyond the ideal ballooning boundary. ITG and ETG modes are generally predicted to be unstable (neglecting  $\omega_{se}$ ). Trapped electrons have been found to be especially important for the modes in the region  $O(1/\rho_i) < k_y < O(1/\rho_e)$  in the L-mode plasma with steeper density gradient. Equilibrium flow shear  $\omega_{se}$  is dominated by sheared toroidal rotation in this region and this generally exceeds the growth rates of longer wavelength modes with  $k_y \rho_i \leq O(1)$  (including ITG), but is less than the growth rates of short wavelength instabilities  $k_y \rho_i > O(1)$  (including ETG). Parallel analyses of NSTX plasmas (NSTX has similar parameters to MAST), also using GS2, give broadly similar findings.

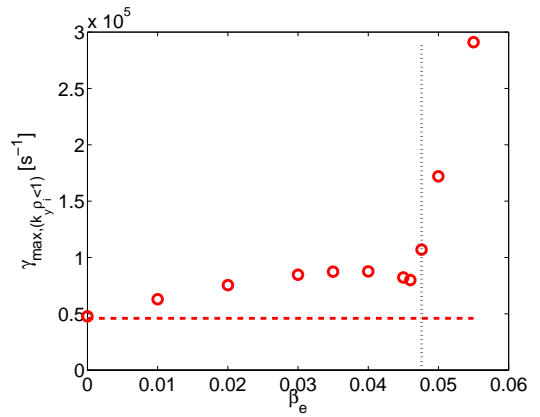


Figure 2: Maximum growth rate for modes with  $k_y \rho_i < 1$  as a function of the electron  $\beta$ ,  $\beta_e$  with the vertical line showing the experimental value. (L-mode,  $\rho_n = 0.5$ ).

## 2.1 Microtearing Modes

GS2 studies of microtearing modes in MAST equilibria [4] have probed the underlying drives. The analytic theory literature highlights two main drive mechanisms for the linear microtearing instability. The first drive mechanism which operates at higher collisionality  $\nu_{ei} > \omega$  (where  $\nu_{ei}$  is the electron-ion collision frequency) is due to the time dependent thermal force driving parallel currents in the plasma, and the second drive mechanism which is more effective at lower collisionality is due to the effect of collisions between trapped and passing particles in a narrow layer of velocity space adjacent to the trapped-passing boundary. Significant parallel currents can be driven by these collisions and carried by the passing particles in this layer, allowing the microtearing instability to grow. Both mechanisms require a finite temperature gradient and an energy dependent collision operator to drive the microtearing instability. Importantly, our calculations using GS2 have shown that neither drive mechanism in the analytic theory literature is crucial to the MAST instability since the mode is largely unaffected when the energy dependence is removed from the collision operator (see Figure 3(a)). Significantly this suggests there must be a further drive mechanism for the microtearing instability. More detailed studies show that the microtearing mode is strongly destabilised by magnetic drifts and the electrostatic potential (see Figure 3(b)). If both of these effects (which are often omitted from analytic theories) are neglected in the calculations, then the MAST instability is completely stabilised. The MAST microtearing mode is unstable in the collisionality range  $0.05 < \nu_{ei}/\omega < 1.2$ , which is an awkward limit for analytic theory since it lies somewhere between the low collisionality and semi-collisional regimes. Analytic treatment of this mode would be further complicated by the width of the current layer which is the order of the ion Larmor radius, requiring that finite Larmor radius effects be included both inside and outside the current layer.

Microtearing modes have also been found in GS2 calculations for large aspect ratio  $s$ - $\alpha$  equilibria at high  $\beta$ . High  $\beta$  enhances the magnetic perturbations that cause the tearing instability and suppresses the ITG mode. Preliminary nonlinear simulations to study the saturation of these instabilities fail to reach saturation due to strongly growing amplitudes of the highest  $k_x$  modes resolved. An explanation for this nonlinear instability is yet to be found.

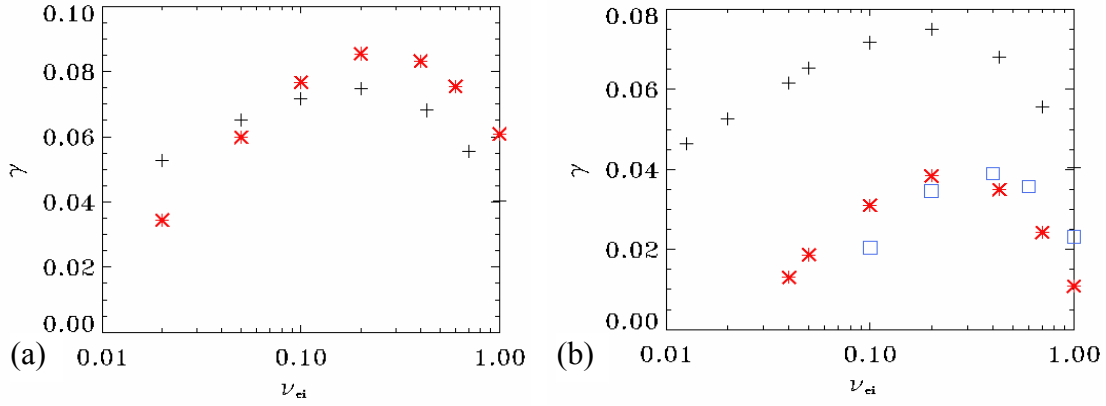


Figure 3: (a) Plots of growth rate  $\gamma$  versus the thermal electron collision rate  $\nu_{ei}$  with (+) and without (\*) energy dependence in the collision operator. (b) Plots of  $\gamma$  versus  $\nu_{ei}$  using various physics models: full physics (+), neglecting the electrostatic perturbation (\*), and finally a model without magnetic drifts (□). If both electrostatic perturbations and magnetic curvature are ignored then the mode is completely stabilised.

## 2.2 Ubiquitous Modes

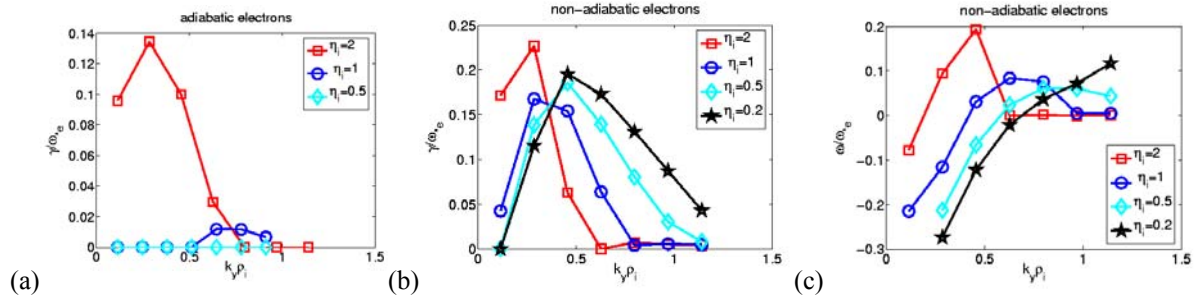


Figure 4: Electrostatic calculation showing  $\gamma/\omega_{*e}$  (where  $\omega_{*e}/\omega_{*i}$  corresponds to the electron/ion diamagnetic frequency) versus  $k_y \rho_i$  for various choices of  $\eta_i$  (a) with adiabatic electrons and (b) including the full electron response. (c) shows the real frequency spectrum corresponding to the calculations shown in (b).

Simpler electrostatic calculations have been performed in the region  $k_y \rho_i \leq O(1)$  for the MAST equilibrium of Fig 1(b), to approach the validity domains of analytic theories, and to study mode sensitivity to the profile parameters  $\eta_j = d \ln T_j / d \ln n_j$  (where  $j$  labels the species).

Assuming an adiabatic response by electrons, instabilities are found with  $\eta_i \sim 2$ . These modes resemble toroidal ITG modes: self-consistent scans (Fig 4(a)) reveal that the mode, which generally propagates in the ion diamagnetic drift direction, is stabilised as  $\eta_i$  falls below 2. On including the full electron response however (see Figs 4(b),(c)), an instability, which now propagates in the electron diamagnetic drift direction, appears as  $\eta_i$  is reduced. This mode is influenced both by trapped electron physics and by ion temperature gradients ( $\eta_i > 0$ ). For sufficiently positive values of  $\eta_i$  ( $\eta_i \geq 0.5$ ) the real frequency of the mode (Fig 4(c)) rises with  $k_y \rho_i$ , and passes through zero close to the peak in  $\gamma/\omega_{*e}$ . The transition from an electron drift mode to a mode propagating in the ion diamagnetic direction was noted in [5], where the ion mode was termed the ubiquitous mode. In the low frequency transition region the mode is a fluid instability driven by ion and electron magnetic drifts in the adverse curvature region. It is closely related to the toroidal ion pressure gradient driven mode, but no longer requires ion temperature gradients to destabilise it, though positive  $\eta_i$  still contributes to instability.

### 3. ITBs and Rotation

#### 3.1 Trapped electron modes in steep plasma profiles

The trapped electron mode can be destabilised by collisions or precessional drift resonances, but the latter effect will be exponentially small in steep density gradients, such as at an internal transport barrier (ITB). In the collisional regime there is an unstable dissipative trapped electron mode (DTEM) for all  $\eta_e$ , but at low collisionalities, using a simple Krook collision operator, one finds stability at long wavelengths ( $b=(k_y \rho_i)^2 \ll 1$ ) for positive  $\eta_e$ . We explore this transition using a pitch-angle scattering collision operator with energy dependent collision frequency,  $\nu_e \sim v^{-3}$ . Magnetic drifts and ion sound effects are neglected, ion FLR effects are retained; to obtain a tractable solution for all collision frequencies we model bounce-averages for trapped particles assuming they are deeply trapped and use a flute-like approximation for the perturbation. In the absence of collisions there is a discontinuity between trapped and passing electron populations (the non-adiabatic contribution to the passing distribution is small because of rapid parallel motion), but collisions resolve this boundary layer. As a result of these approximations one can calculate the perturbed electron density [6].

$$\frac{\hat{n}_e}{n} = \frac{e\phi}{T_e} \left\{ 1 - \frac{8\sqrt{2\varepsilon}}{\pi^{3/2}} \int_0^\infty x^2 e^{-x^2} dx \left[ 1 - \frac{2J_1(a)}{aJ_0(a)} \right] \left[ 1 - \frac{\omega_{*e}}{\omega} (1 + \eta_e(x^2 - 3/2)) \right] \right\}. \quad (1)$$

Equating this to the ion response provides a dispersion relation involving the principle parameters ( $\hat{v} = v_e L_n / v_{thi}$ ,  $b$ ,  $\eta_e$ ,  $\eta_i$ ). At low collisionalities one uses an expansion in  $\nu_e/\omega \ll 1$  to obtain

$$\frac{\gamma}{\omega_{*e}} = \frac{2\Gamma(3/4)}{\pi^{3/2}} \sqrt{\frac{2\nu_e(v_{the})}{\omega}} \left\{ (\eta_i + 1 + \tau)b - \frac{3\eta_e}{4} \right\} \quad (2)$$

implying stability for  $b < b_{crit}(\eta_e)$ . However numerical evaluation leads to the stable region

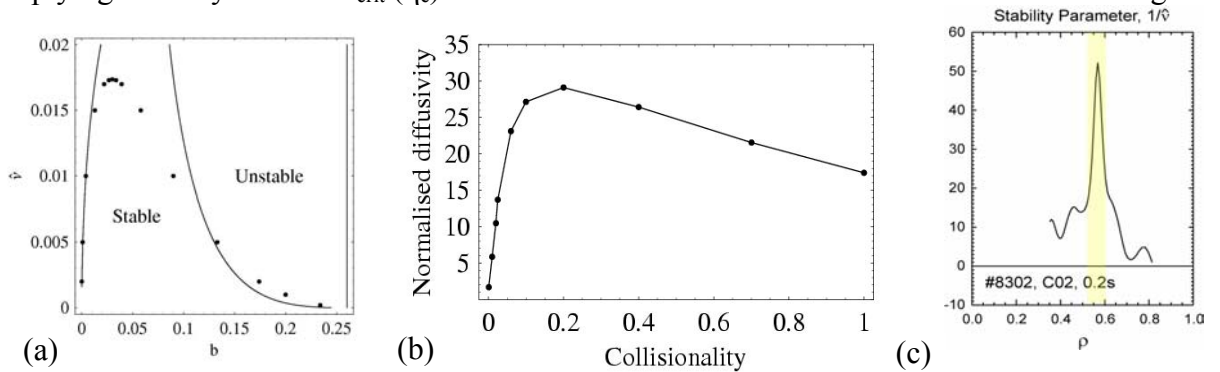


Figure 5 (a) Critical  $\hat{v}(b)$ ; numerical (dots), asymptotic limits (lines); vertical line is given by eqn.(2); (b) Variation of  $\hat{D}$  with collisionality,  $\hat{v}$ ;  $\hat{D}$  reduces sharply at small  $\hat{v}$ ; (c) Experimental values of  $1/\hat{v}$  in a MAST ITB

in the  $\hat{v}$ - $b$  plane shown in Fig. 5(a): the stable region increases with  $\eta_e$ , but decreases, less slowly, with  $\eta_i$ . Below a critical value  $\hat{v} \sim 2-3 \cdot 10^{-2}$ , there is an onset of a stable band of long wavelengths. The fact that this region narrows from the result (2) is because: on the right, the energy dependence of  $\nu_e(v)$  means in some part of the integral (1),  $\nu_e(v)/\omega$  is in the dissipative

regime, while on the left this occurs because  $\omega \propto b^{1/2} < v_e$ . The analytic curve on the right hand side of Fig 5(a) is obtained by evaluating the integral (1) using asymptotic analysis in  $v_e(v_{the})/\omega$ ; the left hand curve corresponds to  $\omega = v_e$ .

It is interesting to estimate the quasi-linear particle flux associated with this instability [7]. Integrating the contribution from the range  $b_{min}(n=1) < b < b_{max} = 1/2$  (the result is relatively insensitive to  $b_{max}$ ) one finds a collisionality dependence shown in Fig 5(b) (the diffusion coefficient  $D$  is normalised to a Bohm-like  $D_0 \sim r\rho_s c_s/L_n$ ). Interestingly the stabilising effect of  $\eta_e$  would imply peaked density profiles. Finally we note that the critical value  $\hat{v} \sim 2-3 \cdot 10^{-2}$  is close to that obtained for MAST ITBs, see Fig 5(c). GS2 is being used to investigate further this possible explanation for ITBs in MAST.

### 3.2 Effect of Sheared Rotation

The collisional transport matrix for a low collisionality plasma with collisional impurity ions has been calculated. The impurities have been found to give rise to off-diagonal terms which can cause the plasma to rotate spontaneously. At conventional aspect ratio the angular momentum flux due to pressure and temperature gradients increases by a factor  $(R/a)^{3/2}$  over previous predictions [8]. It is anticipated that in STs, and for ITBs generally, rotation shear,  $\Omega_q = d\Omega/dq$ , may affect the stability of longer wavelength modes. This problem can be studied using the wave-number representation [9,10] for the perturbation  $\phi(x, k)$ . We consider a generic model where the lowest order solution of the ballooning equation provides a local eigenvalue for the Doppler-shifted frequency  $\omega$  [9]

$$\omega - n\Omega(x) = \lambda(x, k) = \omega_0 - \omega_1 x^2/L_\omega^2 + i\gamma_0 - i\gamma_1 x^2/L_\gamma^2 + \varepsilon \omega_0 \cos k \quad (3)$$

where  $\varepsilon$ ,  $L_\omega$ , and  $L_\gamma$  represent toroidicity and the scale-lengths for the variations in the local  $\omega$  and  $\gamma$ , respectively. This approach reduces the stability problem to the solution of

$$\left[ \frac{1}{\Lambda^4} \frac{d^2}{dk^2} + \omega_q \frac{d}{dk} + \left( \frac{\gamma_0}{\omega_0} - \frac{i(\omega_0 - \omega)}{\omega_0} - i\varepsilon \cos k \right) \right] \Psi = 0 \quad (4)$$

$$\text{where } \Lambda^{-4} = \left[ \frac{\gamma_1}{\omega_0 (nq'L_\gamma)^2} - \frac{i\omega_1}{\omega_0 (nq'L_\omega)^2} \right], \quad \omega_q = \frac{\Omega_q}{\omega_0}, \quad \varepsilon_1 = -i\varepsilon \quad (5)$$

i.e.  $\Lambda^2 = \Lambda_0^2 \exp(-i\alpha)$ ,  $\varepsilon_1 = \varepsilon_0 \exp(i\delta)$ , with  $\Lambda_0 \gg 1$ , where the global eigenvalue,  $\omega$ , is given by requiring periodicity of the solution in  $k$  [10]. This equation has solutions of two types: the conventional ballooning modes localised near  $k = 0$  for small  $\omega_q$ , and 'passing' ones above a critical value of  $\omega_q$ . Using asymptotic matching techniques one can derive analytic formulae to explore this transition. General features of the solution of the dispersion relation are evident analytically. There is normally a continuous evolution of the mode and its complex frequency from the conventional ballooning mode at zero flow shear to a passing mode at high flow shear. The latter mode is essentially cylindrical in its nature, toroidal effects being averaged out by flow shear: consequently it is more stable. The transition becomes sharper as  $\Lambda_0$  (i.e.  $n$ ) increases, defining a critical value:  $\omega_q^{crit} \sim \sqrt{2\varepsilon_1}/\Lambda_0^2 \sim 1/n$ . The degree of stabilisation of a particular harmonic,  $p$ , of the conventional mode depends on which harmonic,  $\ell$ , of the passing modes it links to, the higher harmonics of the latter being more stable. As numerical solutions show, this is a complex question depending on model parameters, e.g. the phase-angle  $\alpha$ . Specific numerical results have been obtained for three special cases. The first is where the radial variation is due entirely to the growth rate ( $\alpha = 0$ ) and the toroidal coupling is in phase with the lowest order frequency,  $\delta = -\pi/2$  (the last condition is typical of drift waves). This shows that the most unstable ( $p = 0$ ) harmonic of the conventional ballooning mode

becomes the more stable passing mode ( $\ell = 0$  – i.e. with zero real frequency but the most unstable passing mode) as  $\omega_q$  increases. The second and third harmonics first coalesce and then acquire real frequencies corresponding to  $\ell = \pm 1$  as they evolve to the more stable passing modes. The second limiting case is when the radial variation is in the real frequency,  $\alpha = \pi/4$ , but  $\delta = -\pi/2$  again. In this case the conventional ballooning modes are essentially unaffected by  $\omega_q$  but the real frequency of the passing modes at zero  $\omega_q$  evolves so as to coalesce with neighbouring ones before returning in a cyclic manner. However this behaviour is not robust to a small change in  $\alpha$ : the real parts then evolve without bound. Finally in Figure 6 we show the variation of growth rate for an intermediate case:  $\alpha = \pi/8$ ,  $\delta = -\pi/4$  where both  $\omega$  and  $\gamma$  vary radially. In this case the lowest harmonic conventional modes link to passing modes with high values of  $\ell$  (and hence are the more stable), whereas it is a higher harmonic that links to the most unstable passing mode,  $\ell = 0$ .

This analysis suggests that rotation shear can be included in GS2 by allowing the ballooning angle  $\theta_0$  to rotate in time and calculating the time-averaged growth.

#### 4. Nonlinear ETG

Nonlinear calculations are required to predict transport arising from microinstabilities. ITG modes are likely to be damped by equilibrium flow shear in MAST as  $\omega_{se} > \gamma_{ITG}$ , but ETG modes should be less affected. GS2's geometry is most appropriate if the flux-tube is sufficiently thin in radius that the equilibrium gradient scale-lengths can be taken as constant.

For these reasons nonlinear GS2 turbulence calculations [11] have focussed on ETG modes. As electromagnetic effects are important at mid-radius in MAST, they are therefore included. Calculations have been undertaken to assess the impact of ETG turbulence on the  $\psi_n = 0.4$  surface ( $\psi_n$  is the normalised poloidal flux) of a MAST H-mode discharge (#6252). These nonlinear computations were carried out on the

HPCx (Daresbury, UK) and Cheetah (Oak Ridge, US) supercomputers and typically take 4-8 wall clock hours on 256 processors. The flux-tube extends 7m along the field line and has perpendicular dimensions  $x=690\rho_e$  and  $y=628\rho_e$ , where  $\rho_e=0.12\text{mm}$ . The grid in  $y$  resolves

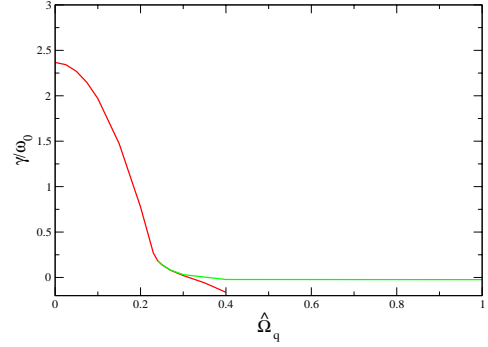


Figure 6: Variation of the normalised growth rate,  $\gamma/\omega_0$ , with increasing flow shear,  $\omega_q$ , for the lowest, most unstable, conventional ballooning mode harmonic,  $p=0$ , for the standard case:  $\Lambda_0^2=15, \epsilon_0=2, \alpha=\pi/8, \delta=-\pi/2, \gamma_0/\omega_0=1$ . In this case  $p=0$  evolves into the most unstable passing harmonic  $\ell = -18$ . The red curve from the left matches the green curve from the right in an overlap region of common validity.

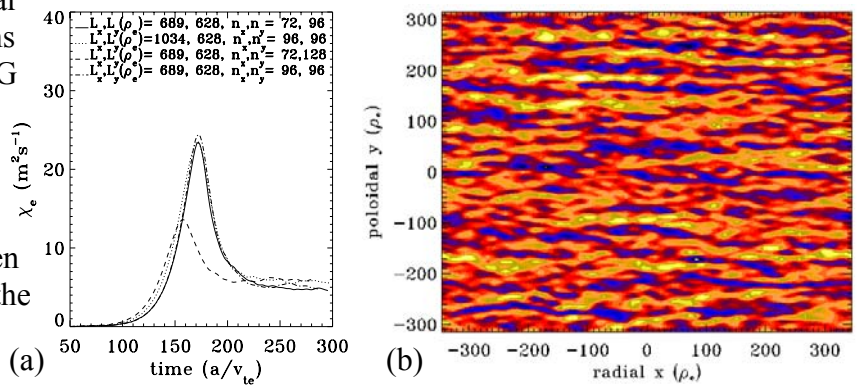


Figure 7: Nonlinear ETG simulations for MAST #6252 at  $\psi_n = 0.4$ . (a) Electron thermal diffusivity as a function of time for various flux-tube resolutions. (b) Contour plot of electrostatic potential in the  $x y$  plane at the intersection of the flux-tube with the outboard equatorial mid-plane.

wavenumbers in the range  $0.01 \leq k_y \rho_e \leq 0.31$ , which includes the most linearly unstable modes. Saturation of the heat flux was observed after  $t = 200a/v_{the}$ , and the electron thermal diffusivity  $\chi_e$  was calculated to be  $\sim 5 \text{ m}^2/\text{s}$ . Convergence has been checked by assessing the sensitivity of the predicted electron heat flux to (i) resolutions in  $x$  and  $y$  (see Figure 7(a)), (ii) including or excluding electron collisions, and (iii) comparing adiabatic ions with including full ion physics. These variations affected the saturated electron transport coefficient by less than a factor of two. The predicted electron thermal diffusivity is much larger than the mixing length estimate ( $\chi_e^{ML} < 0.03 \text{ m}^2/\text{s}$ ). Experimental measurements indicate that  $\chi_e$  lies in the range  $3\text{-}8 \text{ m}^2/\text{s}$  in this region. The GS2 predicted electron thermal diffusivity is experimentally significant, and the enhancement over mixing length predictions appears to be due to the existence of large amplitude, radially elongated streamer structures which are clearly visible in Figure 7(b). More recent work suggests that saturation level of the ETG turbulence is sensitive to the inclusion of trapped electron physics [12].

## 5. Conclusions

The GS2 code, supported by analytic models has been used to identify the instabilities present in the spherical tokamak, device MAST, in particular exploring the effects of high  $\beta$ . Micro-tearing, ITG, ETG, trapped electron modes and the ubiquitous instabilities have been identified. Generic modelling of rotation shear suggests an approach to including it in GS2. Simulations of ETG transport are compatible with  $\chi_e$  in MAST.

## Acknowledgements

This work was funded jointly by the United Kingdom Engineering and Physical Sciences Research Council and by the European Communities under the contract of Association between EURATOM and UKAEA. Supercomputing resources were made available on the US DOE's Cheetah machine at ORNL and on the UK EPSRC's 'HPCx' supercomputer at CCLRC Daresbury under the EPSRC grant GR/S43559/01. The views expressed herein do not necessarily reflect those of the European Commission.

## References

- [1] KOTSCHENREUTHER, M., et al., *Comput. Phys. Commun.* **88** 128, 1995
- [2] APPLGATE, D.J., et al., *Phys. Plasmas*, **11**, 5085, 2004.
- [3] ROACH, C.M., et al., *Plasma Phys. Control. Fusion* **47**, B323, 2005.
- [4] APPLGATE, D.J., et al., 'Microtearing Modes in MAST', *Proceedings of 32nd EPS Conference on Plasma Physics, Tarragona, ECA volume 29C*, P5-101, 2005.
- [5] COPPI, B., PEGORARO, F., *Nuclear Fusion* **17**, 969, 1977.
- [6] CONNOR, J.W., et al., *Plasma Phys. Control. Fusion* **48** 885 (2006)
- [7] CONNOR, J.W., et al., 'Trapped electron mode stability in regions of steep gradients', *Proceedings of 33rd EPS Conference on Plasma Physics, Rome, O3-002*, 2006
- [8] NEWTON, S. HELANDER P., *Phys. Plasmas* **13**, 012505, 2006.
- [9] DEWAR, R.L., *Plasma Phys. Control. Fusion*, **39**, 453, 1977.
- [10] CONNOR, J.W., et al., 'Rotation shear and ballooning modes', *Proceedings of Joint Varenna-Lausanne International Workshop on Theory of Fusion Plasmas, Varenna, 457*, 2004.
- [11] JOINER, N., et al., *Plasma Phys. Control. Fusion* **48**, 685, 2006
- [12] JOINER, N., HIROSE, A., 'Transport enhancing features of ETG turbulence', *Proceedings of 33rd EPS Conference on Plasma Physics, Rome, 2006*.